Environmental Science & Technology

Article

pubs.acs.org/est

Kinetics and Mechanism of the Oxidation of Cyclic Methylsiloxanes by Hydroxyl Radical in the Gas Phase: An Experimental and Theoretical Study

Ruiyang Xiao,[*,†,‡] Ian Zammit,[§] Zongsu Wei,[∥] Wei-Ping Hu,[▽] Matthew MacLeod,[§] and Richard Spinney[*,⊥]

[†]Institute of Environmental Engineering, School of Metallurgy and Environment, Central South University, Changsha, Hunan 410083, China

[‡]Chinese National Engineering Research Center for Control & Treatment of Heavy Metal Pollution, Changsha, Hunan 410083, China

[§]Department of Environmental Science and Analytical Chemistry, Stockholm University, Svante Arrhenius väg 8, Stockholm SE-11418, Sweden

[∥]Department of Civil, Environmental, and Geodetic Engineering and [⊥]Department of Chemistry and Biochemistry, The Ohio State University, Columbus, Ohio 43210, United States

[▽]Department of Chemistry and Biochemistry, National Chung Cheng University, Minxiong, Chia-Yi 62102, Taiwan

Supporting Information

ABSTRACT: The ubiquitous presence of cyclic volatile methylsiloxanes (cVMS) in the global atmosphere has recently raised environmental concern. In order to assess the persistence and long-range transport potential of cVMS, their second-order rate constants (k) for reactions with hydroxyl radical ($^{\bullet}$OH) in the gas phase are needed. We experimentally and theoretically investigated the kinetics and mechanism of $^{\bullet}$OH oxidation of a series of cVMS, hexamethylcyclotrisiloxane (D_3), octamethycyclotetrasiloxane (D_4), and decamethycyclopentasiloxane (D_5). Experimentally, we measured k values for D_3, D_4, and D_5 with $^{\bullet}$OH in a gas-phase reaction chamber. The Arrhenius activation energies for these reactions in the temperature range from 313 to 353 K were small (−2.92 to 0.79 kcal·mol^{-1}), indicating a weak temperature dependence. We also calculated the thermodynamic and kinetic behaviors for reactions at the M06-2X/6-311++G**//M06-2X/6-31+G** level of theory over a wider temperature range of 238−358 K that encompasses temperatures in the troposphere. The calculated Arrhenius activation energies range from −2.71 to −1.64 kcal·mol^{-1}, also exhibiting weak temperature dependence. The measured k values were approximately an order of magnitude higher than the theoretical values but have the same trend with increasing size of the siloxane ring. The calculated energy barriers for H-atom abstraction at different positions were similar, which provides theoretical support for extrapolating k for other cyclic siloxanes from the number of abstractable hydrogens.

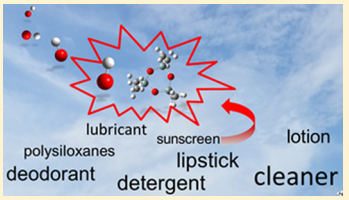

INTRODUCTION

Cyclic volatile methylsiloxanes (cVMS) are widely used in silicon polymer synthesis and personal care products (e.g., lotions and deodorants).[1−6] Nearly 100 million kg of cVMS is produced in the European Union and North America per year.[5,7] Increasing worldwide awareness about the presence of cVMS in the environment has inspired more and more intensive investigations of their environmental behavior and potential risks, which provides scientific background for decision makers for these high-volume chemicals.[7,8]

More than 90% of cVMS emissions are into the atmosphere.[1,3,5] Buser et al.[9] recently measured decamethylcyclopentasiloxane (D_5) and dodecamethylcyclohexasiloxane (D_6) at levels up to 650 and 79 ng·m^{-3}, respectively, in the urban air of Zurich, Switzerland, and most emissions are generally expected to occur in urban areas of industrialized countries. The atmospheric half-lives of cVMS have been estimated to range from days to weeks (e.g., 30 days for hexamethylcyclotrisiloxane D_3, 15 days for octamethylcyclotetrasiloxane D_4, and 10 days for D_5).[3,5,10] The combination of high emission rates and atmospheric half-lives of days to weeks means that cVMS are distributed in the atmosphere at hemispheric scales.[1,11,12] Genualdi et al.[1] reported up to approximately 10 ng·m^{-3} cVMS in the atmosphere in the Arctic, which is about 1−2 orders of magnitude higher than other hydrophobic contaminants, such as polychlorinated biphenyls.

The major degradation pathway of cVMS in the atmosphere is oxidative reaction by hydroxyl radical ($^{\bullet}$OH).[1,12] This pathway produces hydroxylated methyl groups with lower hydrophobicity than the cVMS that can subsequently be

Received: August 3, 2015
Revised: October 9, 2015
Accepted: October 19, 2015
Published: October 19, 2015

DOI: 10.1021/acs.est.5b03744
Environ. Sci. Technol. 2015, 49, 13322−13330

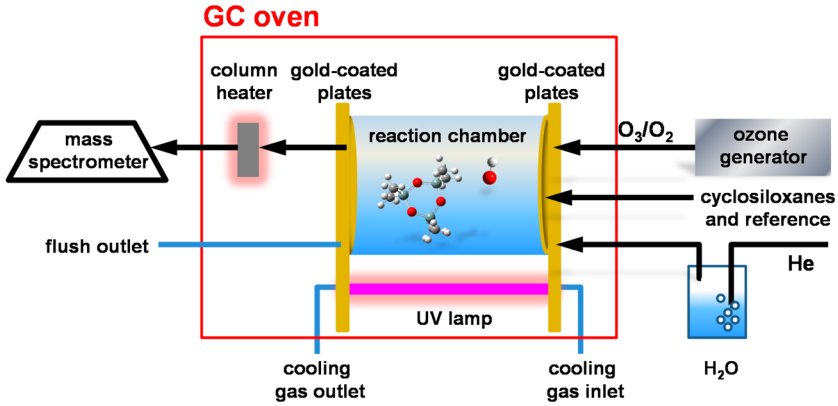

Figure 1. Schematic of experimental setup for gas-phase reaction chamber.

removed from the atmosphere by wet deposition.[6,7] Silicon was recently reported to be a frequently occurring element in atmospheric nanoparticles, suggesting that photochemically transformed volatile methylsiloxanes contribute to aerosol formation in the atmosphere.[13] Atkinson[6] determined the rate constants (k) for gas-phase reactions of D_3, D_4, and D_5 with $^{\bullet}OH$ at 298 K to be $(0.52 \pm 0.17) \times 10^{-12}$, $(1.01 \pm 0.32) \times 10^{-12}$, and $(1.55 \pm 0.17) \times 10^{-12}$ $cm^3 \cdot molecule^{-1} \cdot s^{-1}$, respectively. Sommerlade et al.[14] measured the rate constant for reaction of D_4 with $^{\bullet}OH$ to be $(1.26 \pm 0.40) \times 10^{-12}$ $cm^3 \cdot molecule^{-1} \cdot s^{-1}$ at 297 K and identified products of the reaction through spectrometric and infrared techniques.

In a recent study, Safron et al.[15] measured reaction rates of D_4, D_5, and D_6 with $^{\bullet}OH$ between 313 and 353 K in a small-scale reaction chamber, using the method of relative rates with cyclohexane as a reference substance. The reported k values of D_4, D_5, and D_6 calculated at 298 K from the resulting Arrhenius equations are $(1.9 \pm 0.3) \times 10^{-12}$, $(2.6 \pm 0.3) \times 10^{-12}$, and $(2.8 \pm 0.3) \times 10^{-12}$ $cm^3 \cdot molecule^{-1} \cdot s^{-1}$, respectively.[15] The Arrhenius activation energies for D_4, D_5, and D_6 determined by Safron et al. were not statistically different ($\sim$1.02 $kcal \cdot mol^{-1}$).

There are a number of studies in the literature that employ combined experimental and theoretical approaches to investigate radical and nonradical bimolecular reactions.[16−19] Combining the two methods offers advantages in elucidating reaction mechanisms on the molecular level, especially when reaction channels are competing with each other and/or if there are limitations on the capabilities of analytical tools for product identification. Another possible synergy between experimental and theoretical approaches that has so far not been widely exploited is to provide additional confidence that experimental measurements can be extrapolated to field conditions that are not accessible in the laboratory.

In the present study, we used the same apparatus as Safron et al.[15] to measure k for D_3, D_4, and D_5 between 313 and 353 K, using trimethylpentane (TMP) as a reference substance, which has improved the precision of the measurements (see Experimental Section). In addition, we have theoretically investigated the thermodynamic and kinetic behavior of the reactions using a density functional theory (DFT) method to determine the enthalpies (ΔH_R°), free energies (ΔG_R°), and height of activation energy barrier ($\Delta^{\ddagger} G^\circ$) of the reactions, k, and Arrhenius activation energy for the reaction over a wider temperature range that encompasses the range of temperatures in the troposphere, 238−358 K. Theoretical k values and activation energies are compared to the experimental values, which yields insights about the performance of the theoretical calculations. Finally, the reaction mechanism and potential products of the reaction of the simplest D-series molecule, D_3, with $^{\bullet}OH$ in the reaction chamber are discussed.

EXPERIMENTAL SECTION

Experimental Methods. The gas-phase reaction chamber used in this study has been described previously in detail.[15] A schematic diagram is shown in Figure 1. Briefly, a Thermo Finnigan Trace DSQ gas chromatograph/mass spectrometer (GC-MS) was modified for online sampling of a custom-built reaction chamber. The chamber consists of a 4.2 cm i.d. by 10 cm length quartz glass cylinder (volume 138.5 mL) held in place by two gold-coated stainless steel plates on either side. On the influent side, four openings on the metal plate are used to introduce helium bubbled through water, ozone from an ozone generator (Sander Certizon C300) fed with oxygen, and target compounds. There are two injector ports, one directly on the chamber and the other via a split/splitless GC port. Only one injection port is used at a time. On the effluent side, one port connects the chamber to the MS via a deactivated GC column (Agilent 160-2635-10, 0.10 mm i.d., length 4.5−5 m) that is enclosed in a column heater, while a second port is used as the exhaust. All openings can be closed by valves to render the chamber airtight. The metal plates also hold the UV source (a modified Pen-Ray CPQ 8744, UVP, Cambridge, U.K.) at a distance of 2 cm from one side of the chamber. The chamber is housed inside the GC oven, allowing for measurements at different temperatures.

2,2,4-Trimethylpentane (TMP, Lab Scan, HPLC grade), dichloromethane (Merck, purity 99.8%), D_3 (Sigma−Aldrich, purity 96.0%), D_4 (Fluka, purity 99.0%), and D_5 (Fluka, purity 97.0%) were used as received. Oxygen and helium gases used in the reaction chamber were of 99.6% and 99.999% purity, respectively.

Experimental Measurement. The MS was operated in electron ionization (EI) mode with selected positive-ion monitoring. The ion source and the column heater were kept at 200 and 250 °C, respectively. The fragments to monitor each compound were chosen after individual component runs to rule out interfering peaks of the injected compounds as well as interference from their products with the other analytes and the TMP reference. Degradation due to oxidation by ozone, oxygen, or direct photolysis was excluded by blank runs. Fragments m/z 207, 281, and 355 were chosen for D_3, D_4, and

DOI: 10.1021/acs.est.5b03744
Environ. Sci. Technol. 2015, 49, 13322−13330

D_5, respectively, all of which correspond to $[M^+ - CH_3]$. For the reference compound TMP, m/z 113 $[M^+ - H]$ was chosen.

Mixtures of TMP, D_3, and D_5 in dichloromethane and of TMP and D_4 in dichloromethane (individual concentration range 0.2−0.45 mM) were used for measurements. After the chamber was flushed for 10 min at the temperature of the subsequent measurement, the MS scan was started prior to injection to record background noise for the selected m/z. After about 48 s, an aliquot (1−4 μL) of the mixture was injected directly into the chamber, followed by a period of stabilization in which the components fully volatize and mix in the gas phase, as evidenced by a constant intensity for all peaks. After the MS signal plateau was reached, the UV lamp was turned on to initiate $^{\bullet}$OH production. The UV lamp was turned off after the decay of signals was no longer observed, and the run was stopped approximately 1 min later. The data were imported to MatlabR2014a, and intensity changes were used to calculate the rate constant for the analytes by the method of relative rates as described in Safron et al.[15] The background intensity prior to injection was averaged over time and subtracted from values after injection. The k values for D_3 and D_5 at 40, 60, and 70 °C were measured in quadruplicate. The k values for D_3 and D_5 at 50 and 80 °C were measured five times. The k values for D_4 at 40 and 70 °C were measured in duplicate. The k values for D_4 at 50 °C were measured in triplicate. The k values for D_4 at 90 °C were measured in quadruplicate. The k values for D_4 at 60 °C were measured six times. The k values for D_4 at 80 °C were measured seven times.

The major methodological difference between this study and the study by Safron et al.[15] is that we used TMP as a reference compound instead of cyclohexane. Cyclohexane is a suitable reference compound, but signal interference in the MS with the dichloromethane solvent does not allow monitoring of the molecular ion of cyclohexane at m/z 84. Therefore, a lower fragment of cyclohexane m/z 56 was used in the earlier relative rate measurements reported by Safron et al. Measurements comparing m/z 56 and 84 of cyclohexane showed a small bias in the apparent rate of degradation of 24% (standard deviation of 9%) slower for m/z 56 compared to m/z 84. TMP was chosen as a reference compound since a high fragment, $[M^+ - H]$ at m/z 113, can be monitored.

D_3 Degradation Product Identification. A number of reactions were carried out with the aim of identifying D_3 degradation products by online MS. A reference compound was not used in product identification experiments, since introduction of additional chemicals into the system could obfuscate fragment assignments.

Reaction conditions such as ozone concentration, and hence indirectly the concentration of $^{\bullet}$OH, were varied to identify any differences in responses and reaction products. Tetrachloromethane, CCl_4, which is practically inert to $^{\bullet}$OH, was used as the solvent in these experiments to avoid the possibility of interference from traces of degradation products of dichloromethane. The MS was operated in both full-scan and SIM (selected ion monitoring) modes, and all measurements were conducted at 80 °C. In SIM mode, expected products as well as ions identified through the full scans were monitored. Fragments corresponding to the expected isotopes of silicon (i.e., m/z + 1 and + 2) were also monitored since the relative ratio of these masses gives information on the number of silicon atoms present in the fragment.

Computational Methods. Since the selected cyclosiloxanes have multiple accessible conformations, a conformational search for the global minima of the cyclosiloxanes was performed by use of Spartan'10 with the Merck Molecular Force Field (MMFF) as the molecular mechanics method.[20,21] The conformational search started with 900 initial conformations of each cyclosiloxane by varying Si−O−Si−O torsion angles. Global minima of the cyclosiloxanes and the transition states were then optimized by use of the density functional M06-2X with the 6-31+G** basis set.[22] The term functional means that, with a three-dimensional function of electron density, the energy of a molecule can be uniquely specified. The M06-2X functional used in the current study was developed by Donald G. Truhlar of the University of Minnesota in 2006.[22] Electronic structure calculations were performed with the Gaussian 09 program (Revision A.01).[23−25]

The M06-2X/6-31+G** method was selected in this study because of its high reliability and relatively low computational cost.[22] It has been reported that the performance of the M06-2X functional is reliable for thermochemistry and kinetics for radical oxidation of organic molecules by the developers and other researchers without any prior knowledge of the target compound.[22,26−28] For example, So et al.[26] used the M06-2X functional to study the mechanism and kinetics of $^{\bullet}$OH-initiated oxidation of ethanol. Zhou et al.[27] employed the M06-2X functional to investigate the kinetics of atmospheric photooxidation of 4,4′-dibromodiphenyl ether (BDE-15). They found the theoretical second-order rate constant between BDE-15 and $^{\bullet}$OH was in good agreement with the experimental results.[27] It is noted that M06-2X poorly estimated the kinetics for some chemicals, such as lignin and ethyl formate.[29,30] However, evaluation of the performance of M06-2X functional is beyond the scope of this study. Single-point energies were calculated for the M06-2X/6-31+G** optimized geometries by use of the same functional but with a larger and more flexible basis set, 6-311++G**. Geometry optimizations at the M06-2X/6-311+G** level were attempted but failed. The $\langle S^2 \rangle$ values for the various transition state (TS) structures show minimal spin contamination, ranging from 0.75 to 0.82. For a radical, such as the TS in the current study, S^2 values less than 0.85 are not far from the ideal value of 0.75 [0.5(1 + 0.5) = 0.75], indicating that the spin contamination was minimal. Thus, no artificial corrections are necessary. The nature of all stationary points, either minima or transition states, were examined, and the zero-point energy and thermal contributions to the free energy of activation were determined by calculating the harmonic vibrational frequencies at the M06-2X/6-31+G** level.[31] All of the TS species have one and only one imaginary frequency and no imaginary vibrational frequency for each local minimum. Intrinsic reaction coordinate calculations were performed for all TS species to verify that they were connected between the anticipated reactants and products.[32,33]

All the hydrogen atoms in the optimized cyclosiloxane geometries were grouped on the basis of symmetry. For D_3 (Figure S1), the 18 hydrogen atoms on the optimized molecule were grouped into two categories: axial pointing inward (H10, H14, H18, H22, H26, and H30) and axial pointing outward (H8, H9, H12, H13, H16, H17, H20, H21, H24, H25, H28, and H29). For D_4 (Figure S2), the 24 hydrogen atoms on the optimized molecule were grouped into four categories: equatorial up or down (H24 and H34), equatorial sideways (H22, H23, H35, and H36), axial pointing inward (H12, H16, H20, H28, H32, and H40), and axial pointing outward (H10, H11, H14, H15, H18, H19, H26, H27, H30, H31, H38, and

DOI: 10.1021/acs.est.5b03744
Environ. Sci. Technol. 2015, 49, 13322−13330

H39). For D_5 (Figure S3), the thirty-six hydrogen atoms on the optimized molecule were also grouped into four categories: equatorial up or down (H20, H34, H36, and H45), equatorial sideways (H21, H22, H28, H29, H32, H33, H37, H38, H44, and H46), axial pointing inward (H12, H18, H25, H30, H40, and H49), and axial pointing outward (H13, H14, H16, H17, H24, H26, H41, H42, H48, and H50). A hydrogen atom from each category on the different cyclosiloxanes was selected to react with •OH. For example, for D_3, H18 and H16 were selected as representative hydrogen atoms for axial pointing inward and axial pointing outward positions, respectively; for D_4, H24, H23, H40, and H11 represented equatorial up or down, equatorial sideways, axial pointing inward, and axial pointing outward positions, respectively; and for D_5, H45, H33, H30, and H17 represented equatorial up or down, equatorial sideways, axial pointing inward, and axial pointing outward positions, respectively.

Conventional transition-state theory was employed to model the second-order rate constants ($cm^3 \cdot molecule^{-1} \cdot s^{-1}$) between the select cyclosiloxanes and •OH in the gas phase with 1 atm standard state:[34]

$$k(T) = l\Gamma(T)\frac{k_B T}{h}\exp(-\Delta^{\ddagger}G^{\circ}/RT) \quad (1)$$

where l is the reaction pathway degeneracy (Table S1), the temperature-dependent quantum mechanical tunneling effect $\Gamma(T)$ is corrected by Eckart's method, k_B is Boltzmann's constant, h is Planck's constant, R is the ideal gas constant, and $\Delta^{\ddagger}G^{\circ}$ is the kinetic energy barrier. For reactions involving the transfer of hydrogen atoms, the quantum mechanical effect called tunneling is usually important, and this effect tends to increase the rate constants of the reactions considerably at lower temperature. $Q_{TS}^{\ddagger}$ and Q_R, partition functions for the transition state and reactants, respectively, are included in the $\Delta^{\ddagger}G^{\circ}$ calculation. We assumed that the transition states have no low-lying electronic excited states, and the electronic partition functions of the TS were thus assumed to be 2, independent of temperature. However, due to the low-lying excited states of •OH, the electronic partition function of •OH at different temperatures was calculated as follows:[35]

$$Q_{\bullet OH} = 2 + 2\exp\left(-139.7\frac{hc}{k_B T}\right) \quad (2)$$

where c is the speed of light. The quantity $2/Q_{\bullet OH}$ was multiplied by the rate constants obtained in eq 1. Conventional transition-state theory has been shown to be valid over the temperature range 238−358 K.[36,37]

In most quantum chemical calculations, the approximate solution of the Schrödinger equation is evaluated under the Born−Oppenheimer approximation. The approximation assumes that the energy of the electrons can be evaluated at fixed nucleus positions, and the repulsion between the nuclei can then be added to the electron energy separately. Thus, the energy calculated by this approach is called the Born−Oppenheimer energy, and the Born−Oppenheimer energies at various molecular geometries constitute the potential energy surface on which chemical reactions are usually modeled to take place. We used Born−Oppenheimer energies to delineate the temperature-independent free energy barrier for the first step of •OH oxidation of different cyclosiloxanes.

RESULTS AND DISCUSSION

Experimentally Determined Kinetics. Temperature dependence of the reactions of D_3, D_4, and D_5 with •OH was investigated over the temperature range 313−363 K with TMP as a reference compound, and four experiments were conducted for D_4 at 363 K. To our knowledge, this work represents the first kinetic study of temperature dependence of reaction of •OH with D_3. The measured rate constants are tabulated in Table S2 and illustrated in Figure 2. Extrapolated k

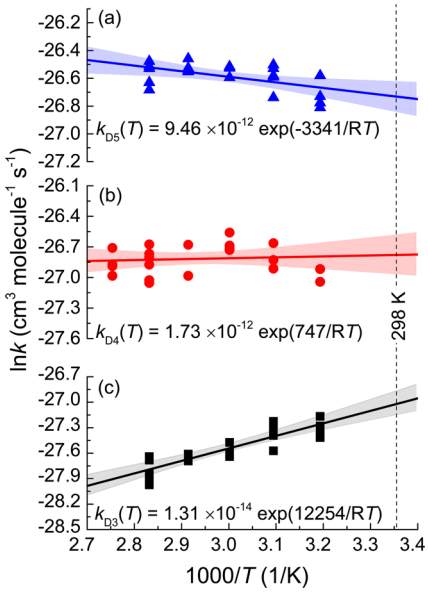

Figure 2. Arrhenius plots of measured gas-phase reaction rate constants k of (a) D_5, (b) D_4, and (c) D_3 with •OH. The central line shows the Arrhenius equation, and the shaded areas indicate 95% confidence intervals of the regression. The vertical dotted line is set at 298 K.

values (with 95% confidence intervals) of D_3, D_4, and D_5 with •OH at 298 K in the gas-phase reaction chamber were $1.84^{1.93}_{1.76} \times 10^{-12}$, $2.34^{2.85}_{1.93} \times 10^{-12}$, and $2.46^{2.74}_{2.20} \times 10^{-12}$ $cm^3 \cdot molecule^{-1} \cdot s^{-1}$, respectively. The measured activation energies (with 95% confidence intervals) are $-2.92^{-2.18}_{-3.67}$, $-0.17^{0.69}_{-1.04}$, and $0.79^{1.38}_{0.21}$ $kcal \cdot mol^{-1}$ for D_3, D_4, and D_5, respectively. Atkinson[6] measured the rate constants for gas-phase reactions of D_3, D_4, and D_5 with •OH at 298 K. Our k values for the cyclosiloxanes at 298 K are higher than the k value at 298 K from Atkinson by a factor of ∼1.6−3.2. We view a factor of 2−3 agreement between studies using different experimental methods as reasonable. For example, Atkinson and Arey[38] reported that k values for a well-studied chemical, propene, varied by up to a factor of ±3 in measurements reported by different laboratories. It is noted that propene is expected to have a similar reaction channel (i.e., H-abstraction) as compared to cyclic methylsiloxanes. The measured k and activation energies for D_4 and D_5 are in very good agreement with previous measurements by Safron et al.,[15] but the precision of our repeat measurements is better when TMP is used as reference substance. The atmospheric half-lives for the cyclosiloxanes, using the measured k at 298 K, are approximately 5.7 days for D_3, 4.5 days for D_4, and 4.2 days for D_5, if a global average •OH concentration of 7.7×10^5 molecules$\cdot cm^{-3}$ is assumed.[39]

We did not observe whether secondary organic aerosols (SOA) were formed in the chamber due to the intense UV light

DOI: 10.1021/acs.est.5b03744
Environ. Sci. Technol. 2015, 49, 13322−13330

during the experiments. We expect products that would be good nucleation points for SOA formation would have low volatility and thus quickly deposit to the walls of the reaction chamber and not interfere with our kinetic measurements

Theoretically Determined Thermodynamics and Kinetics. For D_3, one unique low-energy conformer was identified by the MMFF method,[20] while four conformers were identified for D_4 and eight for D_5 within 1.2 kcal·mol^{-1} of the global minimum. Details are given in Tables S3–S5 in Supporting Information.

The first step of the reaction is abstraction of a methyl hydrogen on the cyclosiloxane molecule via a transition state to form water and cyclosilane-methylene radical.[3,40] The free energy and enthalpy of the reactions were calculated at the M06-2X/6-311++G**//M06-2X/6-31+G** level of theory. Enthalpies, free energies, and heights of activation energy barrier of the H-atom abstraction at 298 K are tabulated in Table 1. Figure S4 delineates temperature-independent Born–

Table 1. Enthalpies, Free Energies, and Heights of Activation Energy Barrier for Reactions of Cyclosiloxanes with •OH[a]

H atom	position	ΔH_R° (kcal·mol^{-1})	ΔG_R° (kcal·mol^{-1})	$\Delta^\ddagger G^\circ$ (kcal·mol^{-1})	BO energy barrier[b] (kcal·mol^{-1})
			D_3		
H16	axial pointing outward	−15.7	−14.5	10.7	2.69
H18	axial pointing inward	−15.7	−14.5	10.1	−0.03
			D_4		
H11	axial pointing outward	−15.8	−14.3	10.6	0.34
H40	axial pointing inward	−16.3	−15.4	10.4	1.09
H23	equatorial sideways	−14.9	−13.9	10.7	0.80
H24	equatorial up or down	−14.9	−13.9	10.4	−0.26
			D_5		
H17	axial pointing outward	−16.3	−16.4	10.7	0.48
H30	axial pointing inward	−15.7	−15.0	10.9	0.96
H33	equatorial sideways	−15.7	−15.9	10.8	0.07
H45	equatorial up or down	−14.9	−14.7	10.4	0.94

[a]Calculated at 298.15 K in gas phase with the M06-2X/6-311++G** level of theory. [b]Zero-point-corrected Born–Oppenheimer (BO) energy barrier.

Oppenheimer energies of reaction and barrier heights of the first step of reactions between different cyclosiloxanes and •OH. Table 1 shows that all of the reactions are thermodynamically favorable processes ($\Delta G_R^\circ < 0$), ranging from −16.4 to −13.9 kcal·mol^{-1}. All the reactions are exothermic (i.e., $\Delta H_R^\circ < 0$), ranging from −16.3 to −14.9 kcal·mol^{-1}. Surprisingly, the heights of activation energy barrier ($\Delta^\ddagger G^\circ$) of the reactions for different cyclosiloxanes are very consistent, ranging from 10.1 to 10.9 kcal·mol^{-1} with a median of 10.7 kcal·mol^{-1}. The consistent $\Delta^\ddagger G^\circ$ for H-atom abstraction reaction on every methyl group on different cyclosiloxane molecules indicates all C–H bond energies on the methyl group are similar and there is little steric hindrance effect for proton abstraction, likely due to the relatively small size of •OH.

Cartesian coordinates for the TS species are tabulated in Tables S6–S15 in Supporting Information. Tunneling correction factors and rate constants k, using Eckart's method for the TS species involved in the reactions with •OH, are tabulated in Table 2. Imaginary frequencies are tabulated in Table S16.

Table 2. Tunneling Correction Factor and Rate Constants for Reactions between Different Cyclic Methylsiloxanes and •OH[a]

H atom	position	tunneling factor	$k \times 10^{-13}$ (cm^3·molecule^{-1}·s^{-1})
		D_3	
H16	axial pointing outward	1.92	0.57
H18	axial pointing inward	4.21	1.61
sum			2.18
		D_4	
H11	axial pointing outward	5.18	1.64
H40	axial pointing inward	1.84	0.43
H23	equatorial sideways	5.11	0.47
H24	equatorial up or down	4.62	0.37
sum			2.90
		D_5	
H17	axial pointing outward	5.62	1.45
H30	axial pointing inward	5.27	0.53
H33	equatorial sideways	5.64	1.18
H45	equatorial up or down	5.05	0.86
sum			4.02

[a]Calculated at the M06-2X/6-311++G**//M06-2X/6-31+G** level of theory at 298 K in gas phase. Tunneling factors were determined by Eckart's method.

The imaginary frequency corresponds to curvature of the potential energy curve around the TS region along the reaction path. Thus, the imaginary frequency is a reasonable measure of width of the potential energy barrier, which is usually the most important factor determining the magnitude of the tunneling effect. Imaginary frequencies for the selected hydrogen atoms on the cyclosiloxanes are similar to a median of −1172.9i cm^{-1}, indicating narrow widths of the potential barriers and, consequently, more pronounced quantum tunneling effects. The corresponding rate constants calculated by Eckart's method for D_3, D_4, and D_5 at 298 K are 2.18×10^{-13}, 2.90×10^{-13}, and 4.02×10^{-13} cm^3·molecule^{-1}·s^{-1}, respectively. The ratio of calculated k for D_3, D_4, and D_5 at 298 K is 1.0:1.3:1.8, which is in good agreement with our experimental values (1.0:1.3:1.5).

When the estimated mean error for activation energy calculation, 1.22 kcal·mol^{-1}, of the M06-2X functional is considered,[22] rate constants calculated by Eckart's correction method are lower than experimental values at the tested temperature range (Figure 3). Other studies also observed this phenomenon.[29] Beste and Buchanan[29] studied the rate constants of α and β hydrogen-atom abstraction of four lignin model compounds with phenoxy and benzyl radicals in the temperature range 580–660 K. Arrhenius plots of all the reactions show that, with similar pre-exponential factors, the M06-2X functional underestimates the Arrhenius activation

DOI: 10.1021/acs.est.5b03744
Environ. Sci. Technol. 2015, 49, 13322–13330

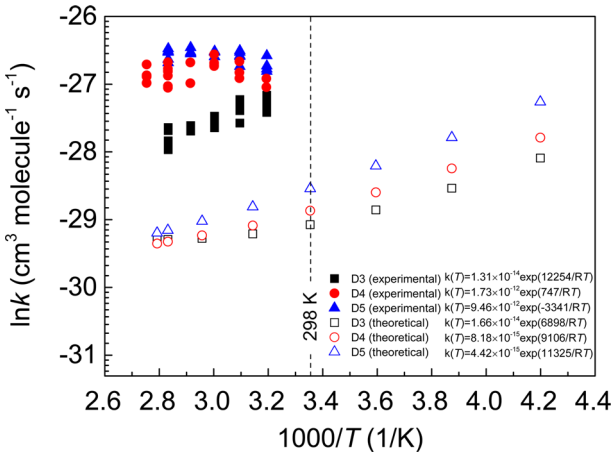

Figure 3. Arrhenius plot of experimental and theoretical rate constants for reactions of cyclic methylsiloxanes with •OH. The vertical dotted line is set at 298 K.

energies by 2.8 and 3.7 kcal·mol^{-1} as compared to experimental values, indicating that M06-2X functional considerably underestimates rate constants. Balaganesh et al.[30] investigated the rate coefficient for reaction of Cl atom and ethyl formate in gas phase over the temperature range 268−343 K. The M06-2X functional systematically underestimates the Arrhenius activation energy by a factor of 2.5, and consequently rate constants are also underestimated. It is noted that our goal was not to reproduce the experimental data and compare their performances. Thus, we did not choose a method that best fits the experimental result. Instead, we kept experimental and theoretical results independent by selecting the most reliable methods available.

Calculated and reported values from the literature at 298 K were also compared.[6,14] Although the rate constants for •OH reactions with D_3, D_4, and D_5 at 298 K can be estimated using EPI Suite with the group contribution method,[41] the EPI Suite estimated k values for the cVMS were not consistent as compared to the values measured by Atkinson.[6]

Xu and Wania[4] reported that the k for the cyclosiloxanes could be empirically described by the number of hydrogen atoms per cyclosiloxane molecule (i.e., k = (0.0858 × numbers of hydrogen − 1.0333)/10^{12}). MacLeod et al.[11] observed a highly positive correlation (R^2 = 0.995) between the number of dimethylated siloxane groups and the k values. They used this correlation to extrapolate the k for D_6 at 298 K. The consistent activation energy barrier height for H-atom abstraction at different positions from our theoretical result indicates that the numbers of hydrogen atoms or dimethylated siloxane groups on the cyclosiloxane molecule are approximately proportional to the rate constants. Thus, our calculations provide a theoretical basis for the empirical relationships between number of hydrogens or number of siloxane groups and k.

Temperature-Dependent Kinetics and Comparison. Experimental and theoretically derived temperature-dependent rate constants for the abstraction of methyl hydrogen on cyclosiloxane molecules by •OH expressed in the conventional Arrhenius equation [$k = Ae^{-E_a/RT}$, where A is a pre-exponential factor, R is the gas constant (8.314 J·K^{-1}·mol^{-1}), and E_a is Arrhenius activation energy in joules per mole] are shown in Figure 3. Similar to other low-barrier H-atom abstraction reactions, the calculated Arrhenius equation displays slightly negative temperature dependence: that is, as temperature increases, k decreases, and temperature has a weak influence on k for this reaction.[42−44] The experimental temperature range (313−363 K) is narrower and slightly higher than the theoretical one (238−358 K) due to limitations imposed by the physicochemical properties of cyclic methylsiloxanes. The chemicals investigated in this study (D_3, D_4, and D_5) are semivolatile, with vapor pressures between 23 Pa (D_5) and 1150 Pa (D_3). At temperatures lower than 313 K, we observed delays in the response of the MS signals to the initiation of •OH production, especially for D_5, which we attributed to partitioning of the chemical to the walls of the reactor system and the capillary column that connects the reactor to the MS (data not shown).

Due to a lack of similar kinetic studies on other cyclic methylsiloxanes, we compared the computational results with compounds that are well-studied. For example, Galano et al.[43] investigated the gas-phase hydrogen abstraction reaction from formic acid by •OH in a temperature range of 296−445 K using different quantum mechanical methods. The negative calculated Arrhenius activation energy is in perfect agreement with the measured one from Singleton et al.[42,43] Galano et al.[44] studied the reaction of a series of hydroxy ethers with •OH via DFT and observed that ethoxymethanol, 2-methoxyethanol, and 2-ethoxyethanol exhibit negative Arrhenius activation energy. The negative Arrhenius activation energy was generally explained by various factors such as prereactant complex, decomposition of energized adduct, and entropic effects.[45−47] We attribute the negative Arrhenius activation energy to entropic effects because of low Born−Oppenheimer barrier (Figure S4), shallow potential well in gas phase, and radical and nonradical bimolecular reactions in nature. The temperature-dependent free energy barriers are tabulated in Table S17. Energy barriers for the selected chemicals decrease as temperature increases.

Reaction Mechanism for Oxidation of D_3. The first step of the reaction of VMS and •OH is H-atom abstraction from the methyl group, producing a D_3 methyl radical and water (Figure 4).[3,40] Subsequent reactions of the D_3 methyl radical, involving consecutive initiation, self-reaction, chain propagation, and isomerization steps, are not clear. We proposed a reaction scheme between D_3 and •OH based on known atmospheric chemistry of similar compounds (Figure 4).[3,14,40,48,49] While a full product characterization of the products is not possible with our instrumentation, the online MS was used to obtain evidence for the expected products. Stable isotopes of silicon (^{28}Si, ^{29}Si, ^{30}Si) were used in the monitoring of fragments, since the distribution of intensities of these different masses gives information on the number of Si atoms in the fragment. It should be noted that nitrogen is absent in our reaction chamber and end products that involve nitrogen atmospheric chemistry cannot take place in our chamber. While this does not affect reaction kinetics, it is expected to affect later products.

The online MS setup did not involve any separation techniques, and only changes over time were monitored. In this setup, observed fragments are due to (1) fragmentation after electron ionization (EI) of D_3 and its first-stage reaction products, (2) fragmentation after EI of nth stage products (i.e., products of the first-stage products of D_3 with •OH, and (3) molecular rearrangements after EI in the MS. The absence of evidence of a particular product in the online MS analysis should not be considered as evidence that the product is not formed. There are many possible reasons that a product could be formed but not detected by the online MS method,

DOI: 10.1021/acs.est.5b03744
Environ. Sci. Technol. 2015, 49, 13322−13330

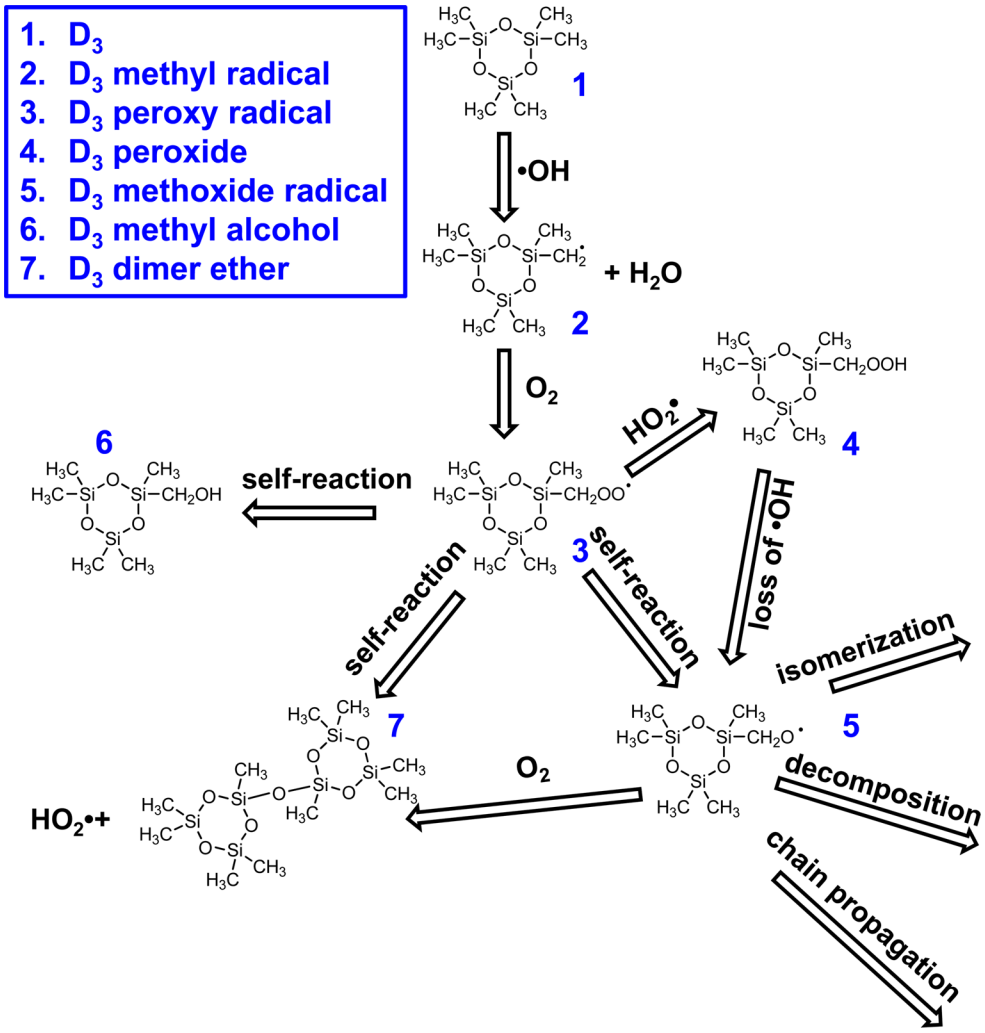

Figure 4. Proposed reaction scheme for D_3 reacting with •OH, based on a similar mechanism for gas-phase chemistry and experimental observations for compounds with similar structure.

including low sensitivity of the detection method and low volatility of the product.

The first step in Figure 4 is formation of D_3 methyl radical and water via H-atom abstraction from a methyl group. In the presence of O_2, the D_3 methyl radical reacts to produce a D_3 peroxy radical. Then there are two possible reaction routes for D_3 peroxy radical: (1) reaction with HO_2• to form a D_3 peroxide, due to barrierless radical−radical reactions,[50,51] or (2) abstraction of an H atom from another methyl group, again forming the peroxide. At this point, in the absence of NO or NO_2, the mostly likely reaction would be the homolytic cleavage of the peroxide O−OH bond to form a •OH and a methoxy radical. The methoxy radical can further react to produce an aldehyde or a D_3 methanol directly or in a multistep process to form a bis(D_3)ether compound; all have been detected experimentally for D_4.[14] Further isomerization, decomposition, and chain propagation reactions are all possible. This reaction scheme is unique compared to those discussed in Sommerlade et al.,[14] which examined the reaction intermediates for D_4 reacting with •OH by GC-MS and GC-FTIR techniques. Our reaction scheme helps to answer whether the detected intermediates are directly derived from oxidation of D_3 or if they are secondary/tertiary/quaternary byproducts. It is noted that the relative importance of different pathways in the reaction chamber may differ from that under tropospheric conditions, since NO and NO_2 can be involved in the tropospheric reactions.

A number of fragments were observed to increase throughout the reaction, such as m/z 193 and 237 in Figure S5. A list of the fragments that clearly increased during the reaction, together with potential molecular assignments, is summarized in Table S18.

The MS data showed strong peaks at m/z 207, which is the molecular ion (M^+) for D_3 with a methyl group removed. This is caused by EI since it is present prior to in situ generation of •OH. Calculations also support this as the loss of a methyl group is endothermic and not likely to occur in normal atmospheric conditions. The m/z 207 intensity decays exponentially after irradiation. Fragments supporting the alcohol and peroxide products have been identified, while the other fragments are nonconclusive and represent fragmentation products of the ring or later-stage decomposition products. For example, fragment m/z 135 is either an advanced degradation product or a lower fragment that has undergone rearrangement. The Si stable isotope distribution for other MS data indicates the presence of several of the compounds proposed in Figure 4. Specifically, the peak at 237.04 would indicate a methyl group converted to a -$CHOH^+$ group. Other peaks indicate the

DOI: 10.1021/acs.est.5b03744
Environ. Sci. Technol. 2015, 49, 13322−13330

presence of a methyl peroxide (-CH_2OOH, peak 239 with the loss of a methyl group due to ionization).

■ ASSOCIATED CONTENT

Supporting Information

The Supporting Information is available free of charge on the ACS Publications website at DOI: 10.1021/acs.est.5b03744.

18 tables showing degeneracies for reactions, measured k values, torsion angles and Cartesian coordinates for TS for D_3, D_4, and D_5, imaginary frequencies, temperature-dependent free energy barriers, and D_3 product fragments; five figures showing optimized geometries for D_3, D_4, and D_5, zero-point-corrected Born−Oppenheimer energies of reactions, and example of PID run for m/z 193 and 237 (PDF)

■ AUTHOR INFORMATION

Corresponding Authors

*(R.X.) Phone +86-731-88830511; fax +86 731-88710171; e-mail xiao.53@csu.edu.cn.

*(R.S.) Phone +1-614-247-6847; fax +1-614-292-1685; e-mail rspinney@chemistry.ohio-state.edu.

Notes

The authors declare no competing financial interest.

■ ACKNOWLEDGMENTS

The research was funded by the Swedish Research Council (VR B0392101). We thank National Natural Science Foundation of China (51474246) and Hunan Provincial Key R&D program (2015WK3014). R.X. gratefully acknowledges Matthew Noerpel for his valuable comments on the manuscript and computing time from the Ohio Supercomputer Center. I.Z. was funded by a Master it! scholarship from the Ministry for Education and Employment, Malta.

■ REFERENCES

(1) Genualdi, S.; Harner, T.; Cheng, Y.; MacLeod, M.; Hansen, K. M.; van Egmond, R.; Shoeib, M.; Lee, S. C. Global distribution of linear and cyclic volatile methyl siloxanes in air. *Environ. Sci. Technol.* **2011**, *45* (8), 3349−3354.

(2) Whelan, M. J. Evaluating the fate and behaviour of cyclic volatile methyl siloxanes in two contrasting North American lakes using a multi-media model. *Chemosphere* **2013**, *91* (11), 1566−1576.

(3) Whelan, M. J.; Estrada, E.; van Egmond, R. A modelling assessment of the atmospheric fate of volatile methyl siloxanes and their reaction products. *Chemosphere* **2004**, *57* (10), 1427−1437.

(4) Xu, S. H.; Wania, F. Chemical fate, latitudinal distribution and long-range transport of cyclic volatile methylsiloxanes in the global environment: A modeling assessment. *Chemosphere* **2013**, *93* (5), 835−843.

(5) Alleni, R. B.; Kochs, P.; Chandra, G. Industrial organosilicon materials, their environmental entry and predicted fate. In *Organosilicon Materials*; Handbook of Environmental Chemistry, Volume 3-*H*; Springer-Verlag: Berlin, 1997; DOI: 10.1007/978-3-540-68331-5_1.

(6) Atkinson, R. Kinetics of the gas-phase reactions of a series of organosilicon compounds with •OH and NO_3 radicals and O_3 at 297 ± 2 K. *Environ. Sci. Technol.* **1991**, *25* (5), 863−866.

(7) Wang, D. G.; Norwood, W.; Alaee, M.; Byer, J. D.; Brimble, S. Review of recent advances in research on the toxicity, detection, occurrence and fate of cyclic volatile methyl siloxanes in the environment. *Chemosphere* **2013**, *93* (5), 711−725.

(8) Rucker, C.; Kummerer, K. Environmental chemistry of organosiloxanes. *Chem. Rev.* **2015**, *115* (1), 466−524.

(9) Buser, A. M.; Kierkegaard, A.; Bogdal, C.; MacLeod, M.; Scheringer, M.; Hungerbuhler, K. Concentrations in ambient air and emissions of cyclic volatile methylsiloxanes in Zurich, Switzerland. *Environ. Sci. Technol.* **2013**, *47* (13), 7045−7051.

(10) Yucuis, R. A. Cyclic siloxanes in air including identification of high levels in Chicago and distinct diurnal variation. Master's Thesis, The University of Iowa, 2013.

(11) MacLeod, M.; Kierkegaard, A.; Genualdi, S.; Harner, T.; Scheringer, M. Junge relationships in measurement data for cyclic siloxanes in air. *Chemosphere* **2013**, *93* (5), 830−834.

(12) McLachlan, M. S.; Kierkegaard, A.; Hansen, K. M.; van Egmond, R.; Christensen, J. H.; Skjøth, C. A. Concentrations and Fate of Decamethylcyclopentasiloxane (D_5) in the Atmosphere. *Environ. Sci. Technol.* **2010**, *44* (14), 5365−5370.

(13) Bzdek, B. R.; Horan, A. J.; Pennington, M. R.; Janechek, N. J.; Baek, J.; Stanier, C. O.; Johnston, M. V. Silicon is a frequent component of atmospheric nanoparticles. *Environ. Sci. Technol.* **2014**, *48* (19), 11137−11145.

(14) Sommerlade, R.; Parlar, H.; Wrobel, D.; Kochs, P. Product analysis and kinetics of the gas-phase reactions of selected organosilicon compounds with OH radicals using a smog chamber-mass spectrometer system. *Environ. Sci. Technol.* **1993**, *27* (12), 2435−2440.

(15) Safron, A.; Strandell, M.; Kierkegaard, A.; MacLeod, M. Rate constants and activation energies for gas-phase reactions of three cyclic volatile methyl siloxanes with the hydroxyl radical. *Int. J. Chem. Kinet.* **2015**, *47* (7), 420−428.

(16) An, T. C.; Gao, Y. P.; Li, G. Y.; Kamat, P. V.; Peller, J.; Joyce, M. V. Kinetics and mechanism of •OH mediated degradation of dimethyl phthalate in aqueous solution: Experimental and theoretical studies. *Environ. Sci. Technol.* **2014**, *48* (1), 641−648.

(17) Ji, Y. M.; Wang, H. H.; Gao, Y. P.; Li, G. Y.; An, T. C. A theoretical model on the formation mechanism and kinetics of highly toxic air pollutants from halogenated formaldehydes reacted with halogen atoms. *Atmos. Chem. Phys.* **2013**, *13* (22), 11277−11286.

(18) DeMatteo, M. P.; Poole, J. S.; Shi, X. F.; Sachdeva, R.; Hatcher, P. G.; Hadad, C. M.; Platz, M. S. On the electrophilicity of hydroxyl radical: A laser flash photolysis and computational study. *J. Am. Chem. Soc.* **2005**, *127* (19), 7094−7109.

(19) Xiao, R. Y.; Wei, Z. S.; Chen, D.; Weavers, L. K. Kinetics and mechanism of sonochemical degradation of pharmaceuticals in municipal wastewater. *Environ. Sci. Technol.* **2014**, *48* (16), 9675−9683.

(20) Halgren, T. A.; Nachbar, R. B. Merck molecular force field 0.4. Conformational energies and geometries for MMFF94. *J. Comput. Chem.* **1996**, *17* (5−6), 587−615.

(21) Shao, Y.; Molnar, L. F.; Jung, Y.; Kussmann, J.; Ochsenfeld, C.; Brown, S. T.; Gilbert, A. T. B.; Slipchenko, L. V.; Levchenko, S. V.; O'Neill, D. P.; DiStasio, R. A., Jr.; Lochan, R. C.; Wang, T.; Beran, G. J. O.; Besley, N. A.; Herbert, J. M.; Lin, C. Y.; Van Voorhis, T.; Chien, S. H.; Sodt, A.; Steele, R. P.; Rassolov, V. A.; Maslen, P. E.; Korambath, P. P.; Adamson, R. D.; Austin, B.; Baker, J.; Byrd, E. F. C.; Dachsel, H.; Doerksen, R. J.; Dreuw, A.; Dunietz, B. D.; Dutoi, A. D.; Furlani, T. R.; Gwaltney, S. R.; Heyden, A.; Hirata, S.; Hsu, C. P.; Kedziora, G.; Khalliulin, R. Z.; Klunzinger, P.; Lee, A. M.; Lee, M. S.; Liang, W.; Lotan, I.; Nair, N.; Peters, B.; Proynov, E. I.; Pieniazek, P. A.; Rhee, Y. M.; Ritchie, J.; Rosta, E.; Sherrill, C. D.; Simmonett, A. C.; Subotnik, J. E.; Woodcock, H. L., III; Zhang, W.; Bell, A. T.; Chakraborty, A. K.; Chipman, D. M.; Keil, F. J.; Warshel, A.; Hehre, W. J.; Schaefer, H. F., III; Kong, J.; Krylov, A. I.; Gill, P. M. W.; Head-Gordon, M. Advances in methods and algorithms in a modern quantum chemistry program package. *Phys. Chem. Chem. Phys.* **2006**, *8* (27), 3172−3191.

(22) Zhao, Y.; Truhlar, D. G. The M06 suite of density functionals for main group thermochemistry, thermochemical kinetics, noncovalent interactions, excited states, and transition elements: two new functionals and systematic testing of four M06-class functionals and 12 other functionals. *Theor. Chem. Acc.* **2008**, *120* (1−3), 215−241.

(23) Frisch, M. J.; Trucks, G. W.; Schlegel, H. B.; Scuseria, G. E.; Robb, M. A.; Cheeseman, J. R.; Scalmani, G.; Barone, V.; Mennucci, B.; Petersson, G. A.; Nakatsuji, H.; Caricato, M.; Li, X.; Hratchian, H.

P.; Izmaylov, A. F.; Bloino, J.; Zheng, G.; Sonnenberg, J. L.; Hada, M.; Ehara, M.; Toyota, K.; Fukuda, R.; Hasegawa, J.; Ishida, M.; Nakajima, T.; Honda, Y.; Kitao, O.; Nakai, H.; Vreven, T.; Montgomery, J. A. J.; Peralta, J. E.; Ogliaro, F.; Bearpark, M.; Heyd, J. J.; Brothers, E.; Kudin, K. N.; Staroverov, V. N.; Kobayashi, R.; Normand, J.; Raghavachari, K.; Rendell, A.; Burant, J. C.; Iyengar, S. S.; Tomasi, J.; Cossi, M.; Rega, N.; Millam, J. M.; Klene, M.; Knox, J. E.; Cross, J. B.; Bakken, V.; Adamo, C.; Jaramillo, J.; Gomperts, R.; Stratmann, R. E.; Yazyev, O.; Austin, A. J.; Cammi, R.; Pomelli, C.; Ochterski, W.; Martin, R. L.; Morokuma, K.; Zakrzewski, V. G.; Voth, G. A.; Salvador, P.; Dannenberg, J. J.; Dapprich, S.; Daniels, A. D.; Farkas, O.; Foresman, J. B.; Ortiz, J. V.; Cioslowski, J.; Fox, D. J. *Gaussian 09*, Revision A.01; Gaussian Inc., Wallingford, CT, 2009.

(24) Becke, A. D. Density-Functional Thermochemistry. III. The Role of Exact Exchange. *J. Chem. Phys.* **1993**, *98* (7), 5648−5652.

(25) Stephens, P. J.; Devlin, F. J.; Chabalowski, C. F.; Frisch, M. J. *Ab initio* calculation of vibrational absorption and circular dichroism spectra using density functional force fields. *J. Phys. Chem.* **1994**, *98* (45), 11623−11627.

(26) So, S.; Wille, U.; da Silva, G. Atmospheric chemistry of enols: A theoretical study of the vinyl alcohol + •OH + O_2 reaction mechanism. *Environ. Sci. Technol.* **2014**, *48* (12), 6694−6701.

(27) Zhou, J.; Chen, J. W.; Liang, C. H.; Xie, Q.; Wang, Y. N.; Zhang, S. Y.; Qiao, X. L.; Li, X. H. Quantum chemical investigation on the mechanism and kinetics of PBDE photooxidation by center •OH: A case study for BDE-15. *Environ. Sci. Technol.* **2011**, *45* (11), 4839−4845.

(28) Xiao, R. Y.; Noerpel, M.; Luk, H. L.; Wei, Z. S.; Spinney, R. Thermodynamic and kinetic study of ibuprofen with hydroxyl radical: A density functional theory approach. *Int. J. Quantum Chem.* **2014**, *114* (1), 74−83.

(29) Beste, A.; Buchanan, A. C., III. Challenges in the computation of rate constants for lignin model compounds. In *Rate Constant Calculation for Thermal Reactions: Methods and Applications*; DaCosta, H., Fan, M., Eds.; Wiley: Hoboken, NJ, 2012; Chapt. 7.

(30) Balaganesh, M.; Dash, M. R.; Rajakumar, B. Experimental and computational investigation on the gas phase reaction of ethyl formate with Cl atoms. *J. Phys. Chem. A* **2014**, *118* (28), 5272−5278.

(31) Ochterski, J. W. *Thermochemistry in Gaussian*; Gaussian, Inc., Wallingford, CT, 2000; http://www.gaussian.com/g_whitepap/thermo.htm.

(32) Fukui, K. The path of chemical reactions - the IRC approach. *Acc. Chem. Res.* **1981**, *14* (12), 363−368.

(33) Dykstra, C. E.; Frenking, G.; Kim, K. S.; Scuseria, G. E. *Theory and Applications of Computational Chemistry: The First 40 Years*; Elsevier: Amsterdam, 2005.

(34) Laidler, K. J. *Chemical Kinetics*, 3rd ed.; Harper & Row: New York, 1987.

(35) Chase, M. W., NIST-JANAF Thermochemical Tables, 4th ed.. *J. Phys. Chem. Ref. Data, Monogr.* **1998**, 9.

(36) Truhlar, D. G.; Garrett, B. C. Variational transition state theory. *Annu. Rev. Phys. Chem.* **1984**, *35*, 159−189.

(37) Garrett, B. C.; Truhlar, D. G. Reliable *ab initio* calculation of a chemical-reaction rate and a kinetic isotope effect: H + H_2 and ^2H + $^2H_2$. *Proc. Natl. Acad. Sci. U. S. A.* **1979**, *76* (10), 4755−4759.

(38) Atkinson, R.; Arey, J. Gas-phase tropospheric chemistry of biogenic volatile organic compounds: A review. *Atmos. Environ.* **2003**, *37*, S197−S219.

(39) Prinn, R.; Cunnold, D.; Rasmussen, R.; Simmonds, P.; Alyea, F.; Crawford, A.; Fraser, P.; Rosen, R. Atmospheric trends in methylchloroform and the global average for the hydroxyl radical. *Science* **1987**, *238* (4829), 945−950.

(40) Markgraf, S. J.; Wells, J. R. The hydroxyl radical reaction rate constants and atmospheric reaction products of three siloxanes. *Int. J. Chem. Kinet.* **1997**, *29* (6), 445−451.

(41) *Estimation Programs Interface (EPI) Suite for Microsoft Windows, v 4.10*; United States Environmental Protection Agency, Washington, DC, 2008.

(42) Singleton, D. L.; Paraskevopoulos, G.; Irwin, R. S.; Jolly, G. S.; Mckenney, D. J. Rate and mechanism of the reaction of hydroxyl radicals with formic and deuteriated formic acids. *J. Am. Chem. Soc.* **1988**, *110* (23), 7786−7790.

(43) Galano, A.; Alvarez-Idaboy, J. R.; Ruiz-Santoyo, M. E.; Vivier-Bunge, A. Rate coefficient and mechanism of the gas phase OH hydrogen abstraction reaction from formic acid: A quantum mechanical approach. *J. Phys. Chem. A* **2002**, *106* (41), 9520−9528.

(44) Galano, A.; Alvarez-Idaboy, J. R.; Francisco-Marquez, M. Mechanism and branching ratios of hydroxy ethers + •OH gas phase reactions: Relevance of H bond interactions. *J. Phys. Chem. A* **2010**, *114* (28), 7525−7536.

(45) Finlayson-Pitts, B. J.; Pitts, J. N. *Chemistry of the Upper and Lower Atmosphere: Theory, Experiments, and Applications*; Academic Press: San Diego, CA, 2000.

(46) Perchyonok, V. T. *Radical Reactions in Aqueous Media*; RSC Green Chemistry, Vol. 6; RSC Publishing: Cambridge, U.K., 2009; DOI: 10.1039/9781849730761.

(47) Singleton, D. L.; Cvetanovic, R. J. Temperature dependence of the reaction of oxygen atoms with olefins. *J. Am. Chem. Soc.* **1976**, *98* (22), 6812−6819.

(48) George, I. J.; Abbatt, J. P. D. Heterogeneous oxidation of atmospheric aerosol particles by gas-phase radicals. *Nat. Chem.* **2010**, *2* (9), 713−722.

(49) Lien, P. Y.; You, R. M.; Hu, W. P. Theoretical modeling of the hydrogen abstraction reaction of fluoromethane by the hydroxyl radical. *J. Phys. Chem. A* **2001**, *105* (11), 2391−2400.

(50) Jasper, A. W.; Klippenstein, S. J.; Harding, L. B.; Ruscic, B. Kinetics of the reaction of methyl radical with hydroxyl radical and methanol decomposition. *J. Phys. Chem. A* **2007**, *111* (19), 3932−3950.

(51) Price, J. M.; Petzold, C. J.; Byrd, H. C. M.; Kenttamaa, H. I. Examination of barriered and barrierless hydrogen atom abstraction reactions by organic radical cations: the cytosine radical cation. *Int. J. Mass Spectrom.* **2001**, *212* (1−3), 455−466.

DOI: 10.1021/acs.est.5b03744
Environ. Sci. Technol. 2015, 49, 13322−13330